Protons with kinetic energy E > 70 MeV trapped in the Earth's radiation belts

E. Fiandrini, G. Esposito, B. Bertucci, B. Alpat, G. Ambrosi, R. Battiston, W. J. Burger, D. Caraffini, L. Di Masso, N. Dinu, M. Ionica, R. Ionica, M. Pauluzzi, M. Menichelli, and P. Zuccon

Department of Physics and Istituto Nazionale di Fisica Nucleare, University of Perugia, Perugia, Italy

Received 17 January 2004; revised 26 April 2004; accepted 14 July 2004; published 28 October 2004.

[1] Accurate measurements of under cutoff proton fluxes in the energy range 0.07–9.1 GeV have been performed with the Alpha Magnetic Spectrometer (AMS) at altitudes of 370–390 km in the geographic latitude interval ±51.7°. A clear transition from a Stably Trapped population typical of the Inner Van Allen belts, in the region of the South Atlantic Anomaly (SAA), to a Quasi-Trapped population in the regions underneath the Van Allen belts outside the SAA is observed. The flux maps as a function of the canonical adiabatic variables L, α_o, and energy E are presented and discussed. *INDEX TERMS:* 2720 Magnetospheric Physics: Energetic particles, trapped; 2768 Magnetospheric Physics: Plasmasphere; 2736 Magnetospheric Physics: Magnetosphere/ionosphere interactions; 2731 Magnetospheric Physics: Magnetosphere—outer; 2716 Magnetospheric Physics: Energetic particles, precipitating;
KEYWORDS: trapped energetic protons, protons in the radiation belts, precipitating protons, protons in South Atlantic Anomoly

Citation: Fiandrini, E., et al. (2004), Protons with kinetic energy E > 70 MeV trapped in the Earth's radiation belts, *J. Geophys. Res.*, *109*, A10214, doi:10.1029/2004JA010394.

1. Introduction

[2] The Van Allen radiation belts start from an altitude of ~320 km over the South Atlantic Anomaly (SAA) and steadily reach the full trapping zone at ~1000 km. This region is well studied, as well as those at high altitude in the atmosphere (~100 km).

[3] The standard model for trapped protons in the Van Allen belts is the AP-8 model, based on the data provided by the long-duration NASA satellite campaigns [*Sawyer and Vette*, 1976; *Vette*, 1991]. This model is de facto the standard against which the other models are compared [*Lemaire et al.*, 1995; *Panasyuk*, 1996; *Beutier and Boscher*, 1995]. Protons models have been developed also by the Institute of Nuclear Physics (INP) of the Moscow State University [*Getselev et al.*, 1991]. Both the AP-8 and INP are static empirical descriptions which describe the average omnidirectional flux in the belts for conditions of minimum and maximum solar activity, in the L shell range between 1.15 and 6.6, with L as defined by *McIlwain* [1961], over a kinetic energy range from 0.1 to 400 MeV.

[4] More recent data are provided by the Combined Release and Radiation Effects Satellite (CRRES) in the energy range 1–100 MeV [*Gussenhoven et al.*, 1993, 1996], by the SAMPEX mission in the range 19–500 MeV [*Looper et al.*, 1996, 1998] and the US TIROS/NOAA polar orbiting weather satellites up to 215 MeV [*Huston et al.*, 1996; *Huston and Pfitzer*, 1998].

[5] Much less is known about the region between the inner Van Allen belts and the atmosphere. One of the major deficiencies in all the existing models is the large uncertainty in the description at low altitudes (<1000 km). Although the principal processes of injection and depletion are known, a complete model of the sources and losses, residence times, the energy spectra and the spatial distribution of the particle populations does not exist. Extensions of existing models to lower altitudes are sensitive to the effects of particle absorption and production in the atmosphere, particularly in the South Atlantic Anomaly region [*Fung*, 1996].

[6] In the atmosphere, the available data come from high-altitude balloon-borne experiments performed in the period 1960–1970 [*Verma*, 1967; *Wenzel et al.*, 1975; *Pennypacker et al.*, 1973], in which the albedo and re-entrant fluxes produced in atmosphere were measured in a energy range from ~45 Mev to ~hundreds of MeV. The major limitation for these experiments is the short duration of the flight.

[7] At energies from ~100 MeV up to the geomagnetic cutoff, high statistics measurements of energetic protons have been performed by AMS in low Earth's orbit [*Aguilar et al.*, 2002]. The study of AMS under cutoff leptons (e^+, e^-) data collected in the same mission are reported elsewhere [*Fiandrini et al.*, 2002, 2003; *Esposito*, 2002]. The study of the lepton fluxes has revealed the existence of a steady population of energetic particles below the classical Van Allen belts with a transition region between a stably trapped population, located in the South Atlantic Anomaly (SAA), and a population of particles generated from and impacting in the atmosphere, charac-

0148-0227/04/2004JA010394

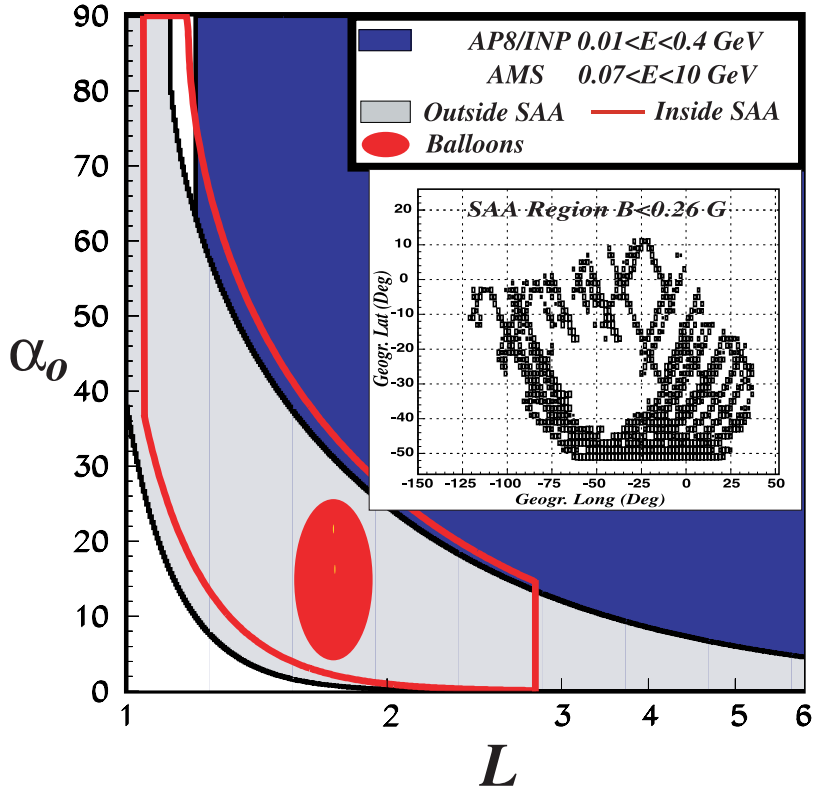

Figure 1. Field of view (FOV) of AMS in the (L, α_o) phase space. The gray area represents the coverage outside the SAA, while the area enclosed by the red curve is the coverage corresponding to the SAA region, defined as the region where $B < 0.26$ G and shown in geographical coordinates in the insert plot. The region with $B < 0.26$ G and its exterior ($B > 0.26$ G) superimpose in the (L, α_o) plane. For comparison, also shown are the coverage of the AP-8 model (blue area) and a typical balloon flight FOV (red region).

terized by residence times up to tens of seconds, in the region below the belts. In this paper, we analyze the proton data to point out the features of the corresponding flux in the same regions.

[8] The AMS data have been analyzed in terms of the canonical invariant coordinates characterizing the particle motion in the magnetic field: the L shell parameter, the equivalent magnetic equatorial radius of the shell [*McIlwain*, 1961; *Hilton*, 1971], and the equatorial pitch angle (α_0) between the momentum $\vec{p}$ and field $\vec{B}$.

2. AMS Data Analysis

[9] AMS was operated on the shuttle Discovery during a 10-day flight, beginning on June 2, 1998 (NASA mission STS-91). The orbital inclination was 51.7° in geographic coordinates, at a geodesic altitude of 370–390 Km. The detector, not magnetically stabilized, recorded data at different fixed attitudes with respect to the local zenith direction (0°, 20°, 45°, and 180°). Details on the detector performance, particle selections and background estimation can be found in [*Aguilar et al.*, 2002] and references therein.

[10] The SAA region is defined using the local geomagnetic field intensity, B, as the region where B < 0.26 G, corresponding to the geographic region shown in the insert of Figure 1. This working definition is commonly used and does not correspond to a physical separation of the drift shells. The data relevant to the present analysis represent 37.5 hours in the region outside of SAA and 8.2 hours in the region of the SAA. The data inside the SAA were not considered in the previous AMS publications. Useful trigger rates varied between 100 and 700 Hz, attaining a maximum rate in the core of the SAA (B < 0.21 G) where the detector livetime went to zero. Data analyzed in the present paper refer to the peripheral regions of the SAA, corresponding to a detector trigger efficiency >90% and livetime >40%.

[11] The values of L, α_0 of the detected protons were calculated using the UNILIB package (TREND Project: http://www.magnet.oma.be/home/trend/trend.html; http://www.oma.be/NEEDLE/unilib.php/20x/; http://www.spenvis.oma.be/spenvis) with a realistic magnetic field model, including both the internal and the external contri-

Table 1. Statistics of the AMS Stably Trapped and Quasi-Trapped Proton Data Used in This Work[a]

	Proton Particle Number	Exposure Time, s
ST Inside SAA	42,806	29,540
QT Inside SAA	87,295	29,540
QT Outside SAA	354,902	135,000

[a]ST, Stably Trapped; QT, Quasi-Trapped. The ST population is permanently trapped above the atmosphere, while the QT one precipitates in the atmosphere within one drift period.

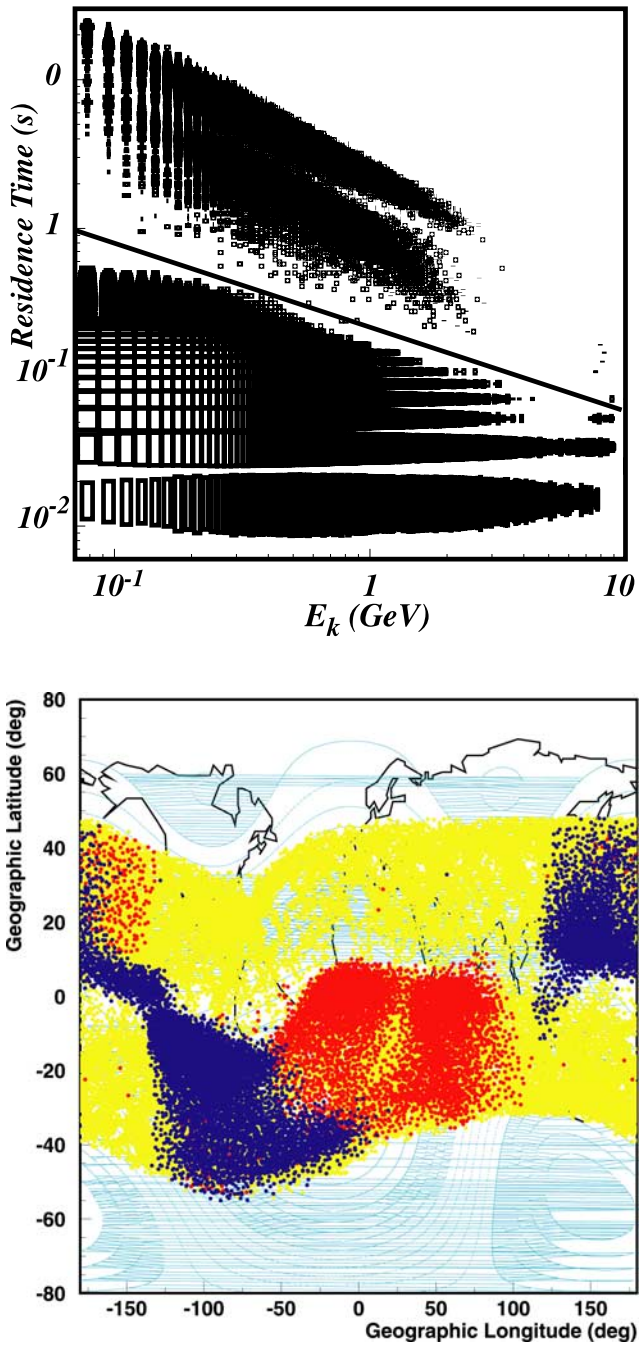

Figure 2. Residence time as a function kinetic energy E for protons in the top plot. The full line shows the curve used to separate the two components. Impact and production points at 40 km a.s.l. for Albedo QT (yellow) and for Proper QT (red and blue), respectively, in the bottom plot.

butions [*Tsyganenko*, 1982] (see http://nssdc.gsfc.nasa.gov/space/model/magnetos/igrf.html). The AMS field of view (FOV) along the orbits is shown in Figure 1, together with the AP8 and typical balloon flight coverages.

2.1. Particle Classification, Residence Times, and Mixed Radiation Belts

[12] To reject the cosmic component of the measured fluxes, the proton trajectories were back-traced in a realistic geomagnetic field model with the Earth's penumbra effects taken into account. Details are reported by *Fiandrini et al.* [2003]. Particles are classified as Cosmic if they reach a distance of 30 Earth's radii. The remaining particles, classified as Trapped, reach the Earth's atmosphere (taken at 40 km a.s.l.) or remain in flight for at least a complete drift around the Earth. These two components are denoted Quasi-Trapped (QT) and Stably Trapped (ST), respectively. Table 1 reports the number of QT and ST secondaries collected by AMS inside and outside the SAA.

[13] To remove possible nonadiabatic behaviors in the trapped proton population, two effective rigidity cutoffs were defined: an upper cutoff R_{cu}, defined as the highest rigidity above which all the protons are cosmic and a lower cutoff R_{cl} as the lowest rigidity below which all the protons are secondaries. The region in between R_{cl} and R_{cu} defines the penumbra region where the adiabatic approach does not hold and the particle motion is not well separated in the three adiabatic periodical motions (gyration, bouncing and drift), with nonlinear dependence on the initial conditions so that the particle classification is uncertain. For this reason, all the particles with $R > R_{cl}$ were rejected even if classified as secondaries from tracing (for more details, see *Fiandrini et al.* [2003]). The adiabaticity conditions were cross-checked with the smallness parameter ϵ [*Il'in et al.*, 1986], which has to be below a critical limit (<0.1); all the particles below the effective cutoff R_{cl} fulfill the condition and have regular adiabatic motion, while all the particles in the penumbra region and the cosmic component have large ϵ values.

[14] The tracing procedure determines the residence times in the belts and the impact and production points (IPP) in the atmosphere for the QT particles (Figure 2). Within the QT population, two components are distinguished as a function of the residence time, T, in the belts. The first one, denoted as Proper QT, is characterized by a residence time scaling with the energy as E^{-1}, limited to energies below ~2 GeV and with IPP points localized in well defined locations corresponding to the weaker regions of geomagnetic field. The second one, denoted as Albedo QT, shows only a weak energy dependence in the residence times, the IPP points are uniformly distributed over two symmetric bands around the magnetic equator and is present at all the energies. Proper QT protons represent ~50% of the undercutoff particle population. This is due to the drift shells, defined as surfaces formed by field line segments such that the first two adiabatic invariants are conserved, mapped out by the different particle types: the albedo QT population moves on shells with most of the mirror points lie below the atmosphere limit (Figure 3a) and will be absorbed in few bounces from the generation; the proper QT (or simply QT) one, instead, follows shells having most of the mirror points above the atmosphere, except in the region of the SAA (Figure 3b) so that they can drift for almost an entire revolution before absorption. The ST particles map drift shells with no points below atmosphere (Figure 3c). The existence of the two populations in the QT components is due to the bouncing loss cone angle, while the ST flux is separated by the drift loss cone angle, as explained in the next section. Such a study points out that at the altitude of 370–390 km, the flux is dominated by particles having residence times much

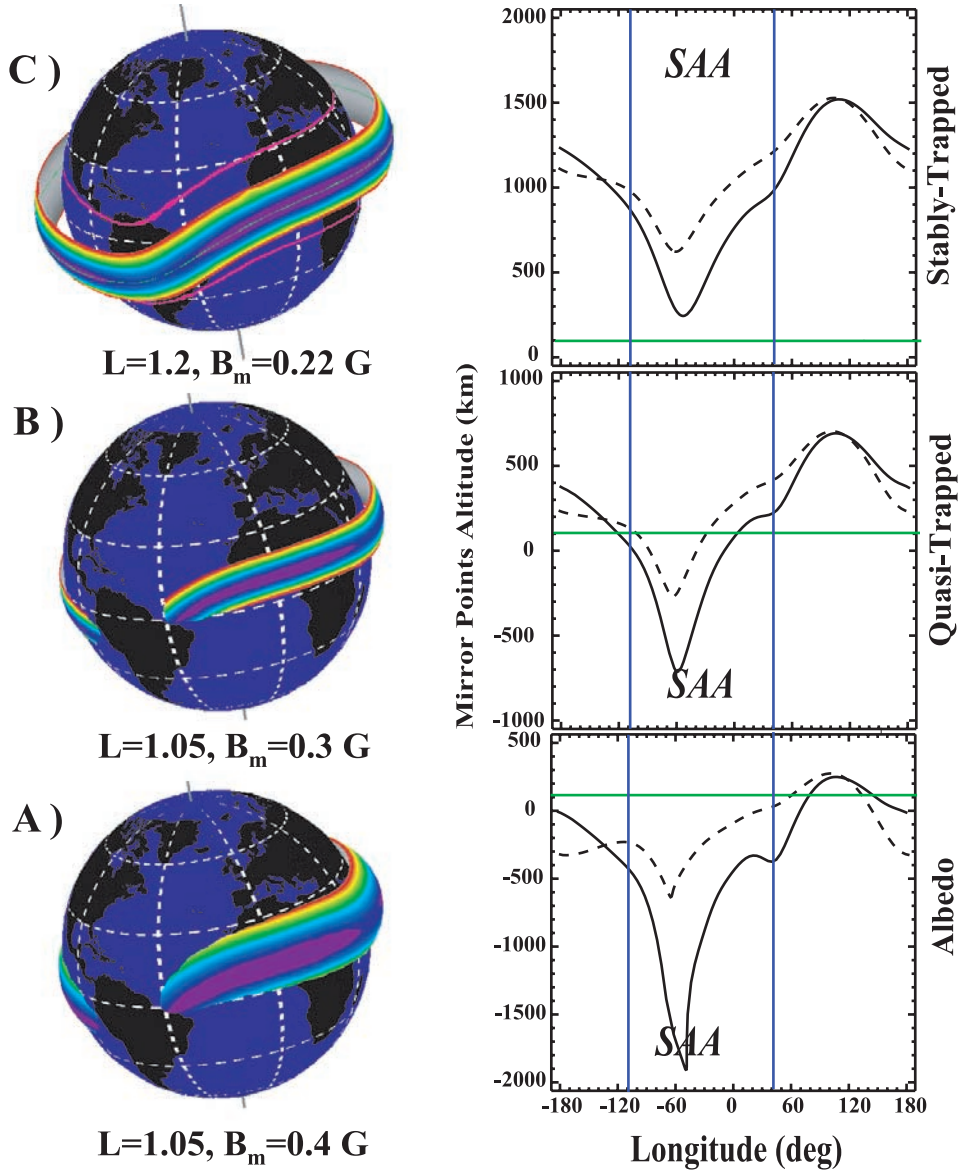

Figure 3. Typical drift shells mapped out by the three different particles populations observed by AMS (see the SPENVIS on-line system at http://www.spenvis.oma.be/spenvis). In the leftmost column, the drift shells surfaces are shown. In the rightmost one, the corresponding altitude of the mirror points (dashed for northern hemisphere, solid for southern hemisphere), in absence of the solid Earth, are shown. The horizontal line represents the atmosphere limit, and the vertical lines denote the SAA region. The ST component (C) has no mirror points below atmosphere limit. The Albedo component (A) has most of its mirror points below the atmosphere, while for the QT component (B) it happens only around the SAA.

shorter than the usual Van Allen belts particles, with an equilibrium between sources and losses in the atmosphere. We use the empirical relation $T_{sep} = 0.25/\sqrt{E}$ to identify the two QT populations. A similar pattern for residence times and IPP was found for leptons [*Fiandrini et al.*, 2002].

[15] The fraction of the ST component was defined as the ratio between the ST flux in the region where $B < B_{SAA}$, the B field value used to define the SAA region, integrated over all the energies and directions, $J^{(ST)}_{B<B_{SAA}}$, and the corresponding total flux of ST and QT particles, $J^{(ST+QT)}_{B<B_{SAA}}$, as a function of B_{SAA}: for a given value of B_{SAA}, the fluxes $J^{(ST)}_{B<B_{SAA}}$ and $J^{(ST+QT)}_{B<B_{SAA}}$ were calculated and the fraction defined as $F_{ST}(B_{SAA}) = J^{(ST)}_{B<B_{SAA}} / J^{(ST+QT)}_{B<B_{SAA}}$.

[16] The fraction of Stably Trapped proton component, F_{st}, can be described with the expression $F_{ST} = 1 - (B_{SAA}/B_o)^{-\alpha} + (B_{SAA}/B_o)^{-\beta}$, with $B_0 = 0.21 \pm 0.01$ G, $\beta = 0.86 \pm 0.07$ and $\alpha = 8.6 \pm 0.2$. B_o is the field value at which the flux becomes entirely stably trapped ($F_{ST} = 1$) and represents the limit of the full Van Allen belts at the altitude of the AMS orbit. The proton transition profile in Figure 4 is less steep than seen for leptons, shown in the same figure, ($B_0 = 0.21 \pm 0.01$, $\beta = 0.59 \pm 0.09$ and $\alpha = 10.7 \pm 0.7$), which suggests a possible difference in the process of

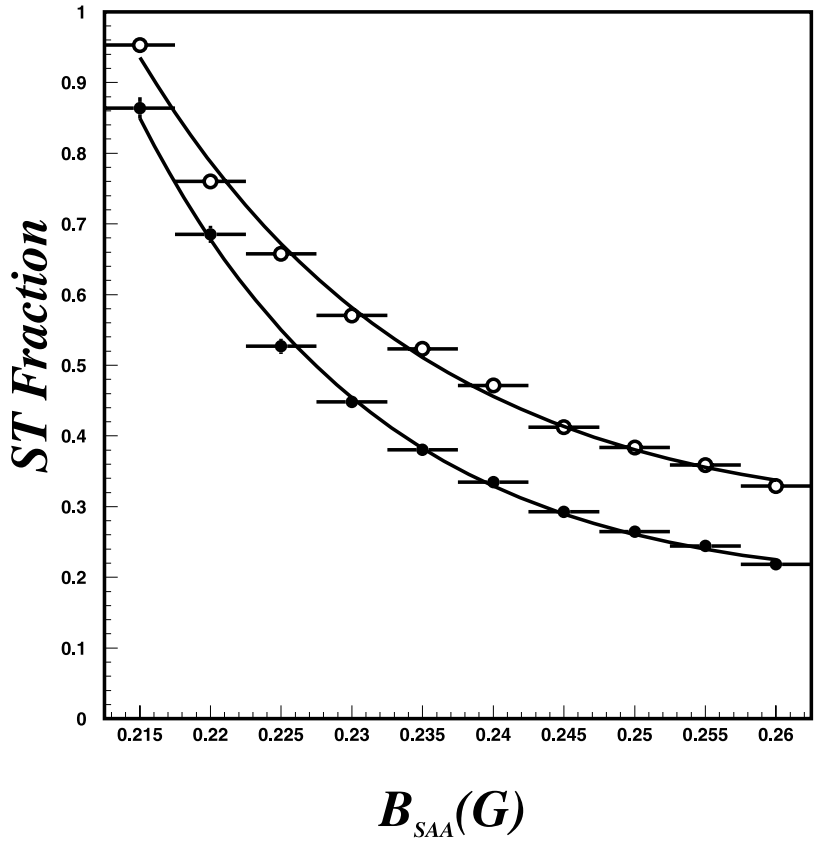

Figure 4. The fraction of Stably Trapped protons (open circles) and leptons (solid circles) as a function of the maximum local magnetic field B_{SAA}, used to define SAA contours. The power law used for the fit is superimposed to the data points.

production and injection for the two types of particles. The two fitted curves converge to the same limit, B_o, of the full Van Allen belts, as expected.

[17] The low detector trigger efficiency in the SAA limits the observable field to B > 0.21 G. Therefore we cannot observe the full canonical Van Allen belts, which do not have drift shells intercepting the atmosphere, but rather the transition region between them and the underlying region, where not closed drift shells, in the sense that they intercept the atmosphere, and Van Allen shells coexist in the region the SAA, which we refer to as the proton Mixed Radiation Belt (MRB).

3. AMS Results

[18] The kinetic energy E, the L-shell parameter and the equatorial pitch angle α_0 are used to describe the fluxes. The pitch angle is preferred to the mirror field value, B_m, since limited to $0°-90°$. A three-dimensional grid (E, L, α_0) is defined for flux maps.

3.1. Integral Flux

[19] Flux maps as a function of (L, α_o) are shown in Figure 5 and as a function of L in Figure 6, over two kinetic energy intervals.

[20] In both the energy intervals the QT fluxes inside and outside SAA look similar and have comparable intensities (Figures 5b, 5c, 5e, and 5f). The integral fluxes at low energy cover the full (L, α_0) phase space accessible to AMS, while at higher energies, the flux at high L and low α_0 is absent both inside and outside the SAA. The similarity of the QT fluxes observed inside and outside the SAA and the different behavior of the ST flux are evident also in the radial distributions presented in Figures 6b, 6c, 6e, and 6f.

[21] The data indicate that the same QT population is observed in different locations of the same drift shells inside and outside the SAA.

[22] The dash-dotted line in Figures 5b, 5c, 5e, and 5f identifies the lower boundary in (L, α_0) below which no Proper QT protons are found. It is defined by the relation $\sin \alpha_b = AL^{-\gamma}$ with A = 0.84 ± 0.03 and γ = 2.82 ± 0.1. The motion of protons with equatorial pitch angles below (above) α_b is dominated by the bouncing along (drifting normal to) the magnetic field line. It can be defined as the equatorial bouncing loss cone for the protons at the altitude of AMS. Taking into account that the particles have regular adiabatic motion, the residence times can be written as a function of the bouncing, τ_b, and drift, τ_d, periods of a particle in a dipolar field in which $\tau_b \sim L/\beta$ and $\tau_d \sim 1/LE_kT = k_d\tau_d\Theta(\alpha_o - \alpha_b) + k_b\tau_b\Theta(-\alpha_o + \alpha_b)$, with Θ the Heavyside function, τ_d, τ_b the drifting and bounce periods, respectively and $k_b \leq 5$, $k_d < 1$ the number of north-south bouncings and the fraction of a complete drift, respectively.

[23] A different behavior characterizes the ST component shown in Figures 5a and 5d. The solid lines represent the lower limit for the Stably Trapped component at the altitude of AMS, described with the relation $\sin \alpha_{st} = BL^{-\beta}$, with B =

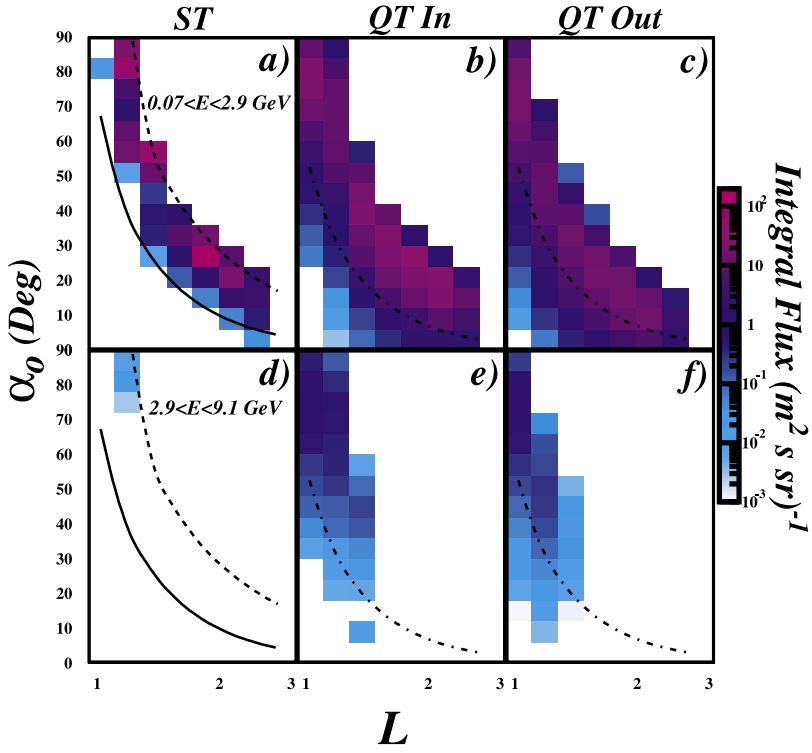

Figure 5. Proton integral flux in the energy interval 0.07–2.9 GeV: (a) for ST, (b) QT in SAA, and (c) QT outside the SAA; integral flux in the interval 2.9–9.1 GeV: (d) for ST, (e) QT in SAA, and (f) QT outside the SAA. In Figures 5a and 5d, dotted curves show the limit for the full Van Allen belts; the solid line shows the equatorial drift loss angle for stable trapping at AMS altitude. The dotted lines in Figures 5b, 5c, 5e, and 5f show the equatorial bouncing loss angle for Proper QT.

0.97 ± 0.05 and $\beta = 1.76 \pm 0.12$. This represents the limit for stable trapping of protons in the IVA belts, meaning that particles with $\alpha_o < \alpha_{st}$ cannot be injected into the IVA belts because all the drift shells intercept the atmosphere; therefore the angle α_{st} can be defined as the equatorial drift loss cone angle. The dashed lines correspond to the limit for the IVA belts at the altitude of AMS, given by $\sin\alpha_{IVA} = \sqrt{0.311/B_o L^3}$, with $B_o = 0.21$ G, the fitted value for ST fraction F_{st}. The region in between the two curves represents the MRB region at the altitude of AMS.

[24] At energies above 2.9 GeV, the ST flux is nearly zero and concentrated at L < 1.1. The absence of ST flux above 2.9 GeV represents an important model constraint. At lower energies, the ST flux shows a dependence on L and α_0 (Figures 6a and 5a), with two maxima at (L, α_0) ~ (1.1, 90°) and ~(1.7, 30°) and a minimum at ~(1.4, 60°).

[25] The local pitch angle, α_l, distribution over the two energy intervals, in Figure 7, shows a difference between ST and QT and a similarity between QT fluxes inside/outside SAA. The ST component (a, b) is strongly peaked at $\alpha_l = 90°$, as expected for locally mirroring, stably trapped particles. A different behavior characterizes the QT (c, d) component, which has a much broader peak with no cutoff, indicating that no stable trapping is possible.

[26] The systematic errors in the particle classification and flux rates, induced by the experimental uncertainties (as the momentum and direction resolution and energy losses in the detector) on the initial conditions of the particles are of the order of few percent and do not give bias in the fluxes. Details are given by *Fiandrini et al.* [2003].

3.2. Differential Flux

[27] Corresponding similarities between QT fluxes inside/outside SAA and differences among QT and ST fluxes observed in the SAA are present also in their spectral behavior. In Figures 8 and 9, the differential flux is shown as a function of (L, α_o) and L, respectively in three intervals of the kinetic energy E and in Figure 10 the differential flux as a function of kinetic energy E is shown in three intervals of L.

[28] The QT differential flux has the same structure in all the phase space and at all the energies, as seen in Figures 8a–8f and in Figures 9a–9f. At equatorial regions, the flux inside and outside SAA is at same level, while with increasing L values the QT flux outside the SAA tends to be softer. This suggests again that the QT fluxes collected inside and outside the SAA are the same particle population observed on different points of the drift shell. Hence we drop the distinction between QT inside and outside the SAA in the following discussion.

[29] The QT flux has an almost flat radial distribution, covering narrower and narrower (L, α_o) regions with increasing energy as a consequence of the geomagnetic cutoff. For the same reason the energy spectra are steepening with increasing L values, Figures 10a–10c.

[30] The ST differential flux shows a different profile with two maxima and a slot which is maximal at low

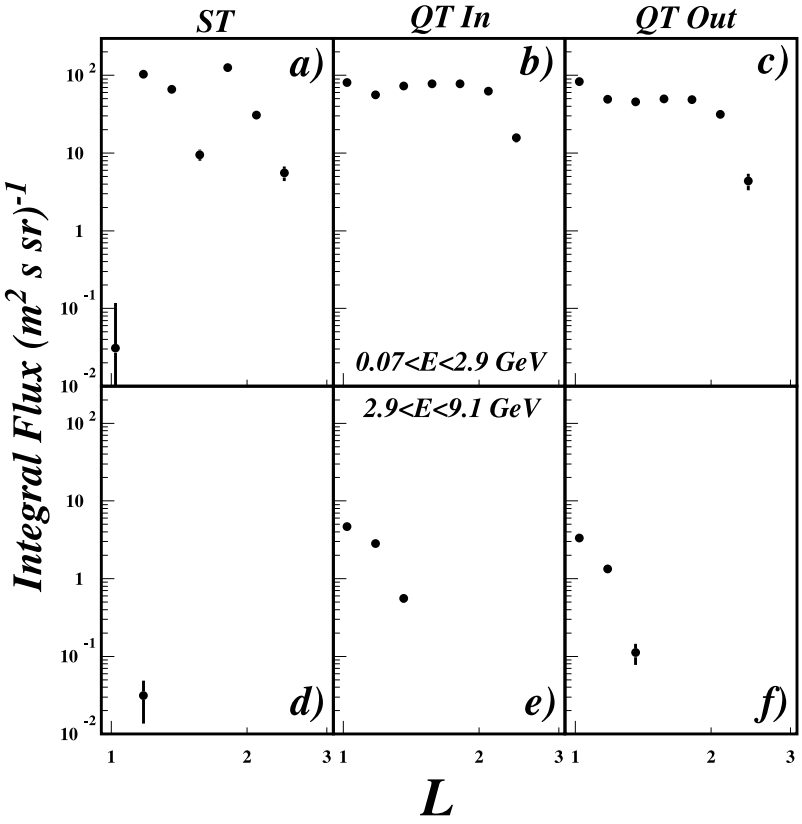

Figure 6. Radial profile of the flux integrated over α_0 in the energy interval 0.07–2.9 GeV is shown for (a) ST and (b) QT components in SAA and (c) QT flux outside SAA and in the interval 2.9–9.1 GeV for (d) ST and (e) QT in SAA and (f) QT outside.

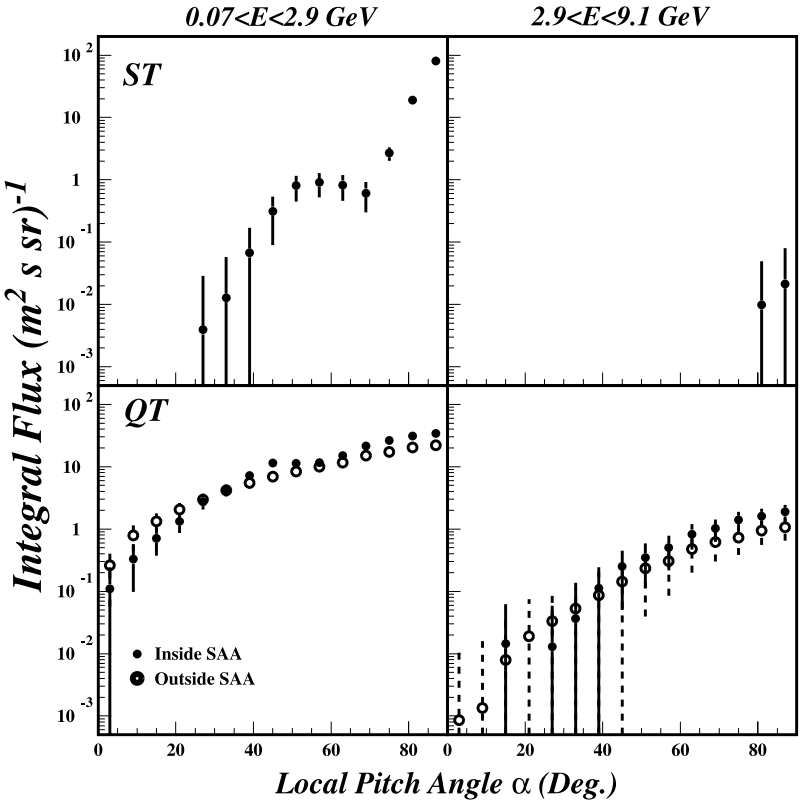

Figure 7. Integral flux in the energy intervals (a and c) 0.07 < E < 2.7 GeV and (b and d) 2.7 < E < 9.1 GeV as a function of the local pitch angle, α, for the (a and b) ST and (c and d) QT protons.

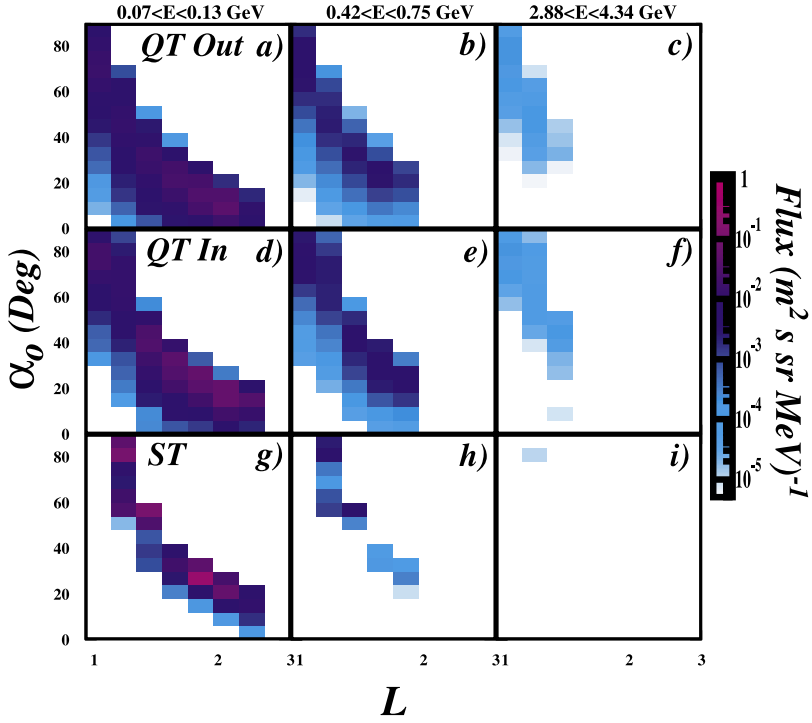

Figure 8. Differential flux maps as a function of (L, α_o) at constant energy in three different energy intervals. Figures 8a, 8b, and 8c show the QT flux outside SAA, Figures 8d, 8e, and 8f show the QT flux inside the SAA, and Figures 8g, 8h, and 8i show the ST flux.

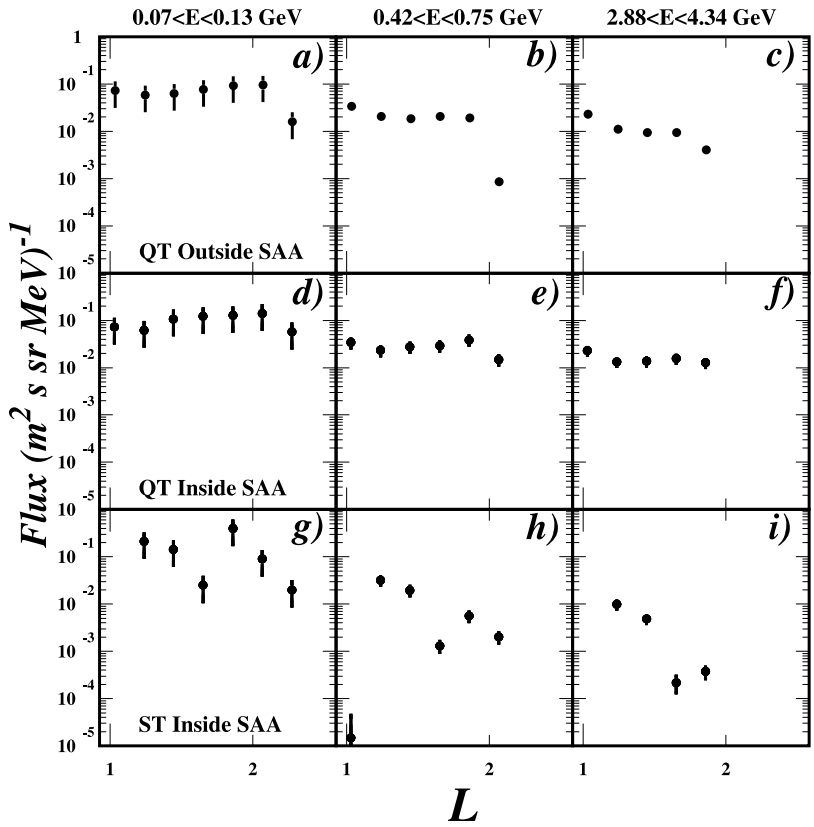

Figure 9. Differential flux as a function of L at constant energy in three different energy intervals. Figures 9a, 9b, and 9c show the QT flux outside SAA, Figures 9d, 9e, and 9f show the QT flux inside the SAA, and Figures 9g, 9h, and 9i show the ST flux.

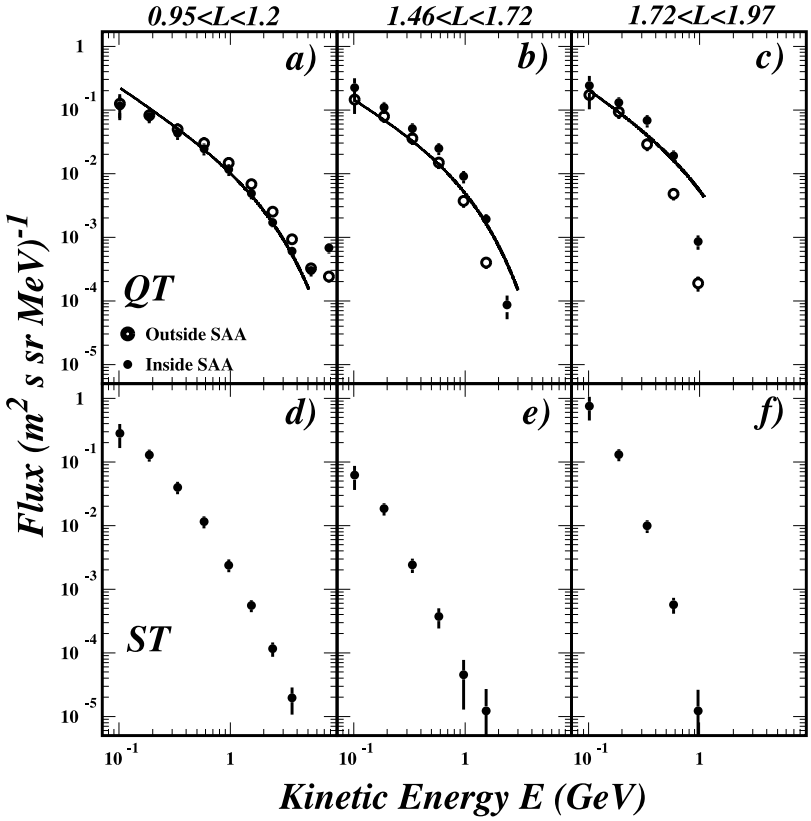

Figure 10. Differential flux maps as a function of kinetic energy E in three different L shell intervals. The lines superimposed to the data show the expected trapped flux from atmospheric production [*Zuccon*, 2002].

energies and vanishes with increasing energy, as shown in Figures 8g–8i and 9g–9i. Compared to the QT flux, the ST component is considerably softer and almost absent above few GeV as shown in Figures 10g–10i, another indication of an energy limitation for the stable trapping in the Van Allen belts.

[31] In Figure 10, superimposed to the QT flux, it is also shown the trapped flux obtained from the 3D Monte Carlo simulation of the interactions of the cosmic rays with the Earth's atmosphere and the subsequent geomagnetic processes [*Zuccon*, 2002; *Zuccon et al.*, 2003]. The results clearly show that the observed QT flux is consistent with an atmospheric production in the interactions of primary helium and hydrogen nuclei.

[32] A more detailed comparison is shown in Figure 11, where the equatorial QT flux is compared with the simulation, together with a prediction from [*Ray*, 1962, 1967] and the flux provided by the AP-8 model (Figure 11a). In the same plot it is also shown a comparison with balloon data measuring the splash and re-entrant albedo particles at ~3–5 gr/cm^2 of residual atmosphere, observed at a magnetic latitude of 41°N (Figure 11b). The observed QT flux is explained by a production process in the interactions of cosmic rays with atmosphere and it is consistent with the Ray calculation. The fluxes measured with balloon-borne experiments in the atmosphere agree very well with those observed at the AMS altitude. Differences up to five orders of magnitude are observed with respect to the AP-8 flux. This is due to the fact that AP-8 model holds only in regions where the local magnetic field is B < 0.21 G, corresponding to the full Van Allen belts, while the AMS data refer to regions where B > 0.21 G and therefore the two sets of data are not directly comparable. However, it is important to note that the flux intensity decreases rapidly as we move from the Van Allen belts to the edge regions outside.

[33] For the ST flux, the relevant difference in the flux slope compared to the QT flux suggests that ST particles might have a different origin, e.g., high-energy Cosmic Ray Neutron Decay, pitch angle diffusion [*Shultz and Lanzerotti*, 1974; *Albert et al.*, 1998] or different geomagnetic transport inside the SAA.

3.3. East/West Asymmetry and (R_m, Λ_m) Maps

[34] Magnetic east/west asymmetries in the QT and ST integral fluxes have been also investigated. In fact, at low altitudes, such asymmetries have been observed in trapped protons at low energy [*Heckman and Nakano*, 1963; *Kruglanski and Heynderickx*, 1999].

[35] By using a local magnetic azimuthal angle, β_o [*Kruglanski and Heynderickx*, 1999], particles from west (east) have always $\beta_o < 0$ ($\beta_o > 0$).

[36] The east/west flux asymmetry A, defined as $A = (J_{\beta_o<0} - J_{\beta_o>0})/(J_{\beta_o<0} + J_{\beta_o>0})$, J being the flux, is shown as a function of L for QT and ST proton components in Figure 12 in the two energy intervals 0.07 < E < 2.9 and 2.9 < E < 9.1 GeV. For the QT flux in the lower energy interval, the asymmetry is compatible with zero within the errors (full dots in the left plot of Figure 12); at higher energy, the

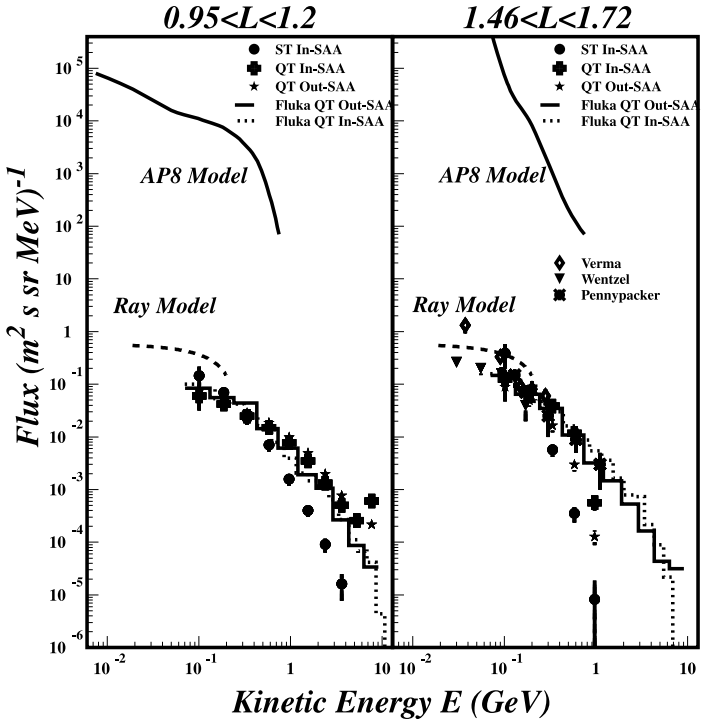

Figure 11. Energy spectrum comparison (a) between AMS, AP8, and Fluka simulation for protons at $0.95 < L < 1.2$ and (b) between AMS, AP8, Fluka, and balloon data for $1.4 < L < 1.72$.

asymmetry is more pronounced with the maximum at equator and decreases with increasing L values (empty dots in right plot of Figure 12). Conversely, the ST fluxes are anisotropic at all the energies with an excess of westward ($\beta_0 > 0$, $A < 0$) protons; for low-energy ST particles the asymmetry is maximal at equator and tends to zero at large L values as expected from geomagnetic cutoff effects, while the flux is strongly suppressed at high energy.

[37] The east/west asymmetry originates from the fact that protons from east have the guiding center below the observation point and experience more atmospheric drag compared to those coming from west with guiding center above it. The drag depends both on the gyroradius, ρ, increasing with energy, and on the residence time, T. For low energy QT particles, both ρ and T are small for relevant interactions with the residual atmosphere [*Walt*, 1964; *Shultz and Lanzerotti*, 1974]; therefore no asymmetry is expected. At higher energies, ρ is large enough to bring the QT particles from east in the more dense atmosphere and a large asymmetry is observed at the equator. For the low-energy ST particles, ρ is small but T is large, so that atmospheric interactions partly remove particles from east and asymmetry shows up. At high energy, where the flux has low intensity and is present only for L < 1.1, both ρ and

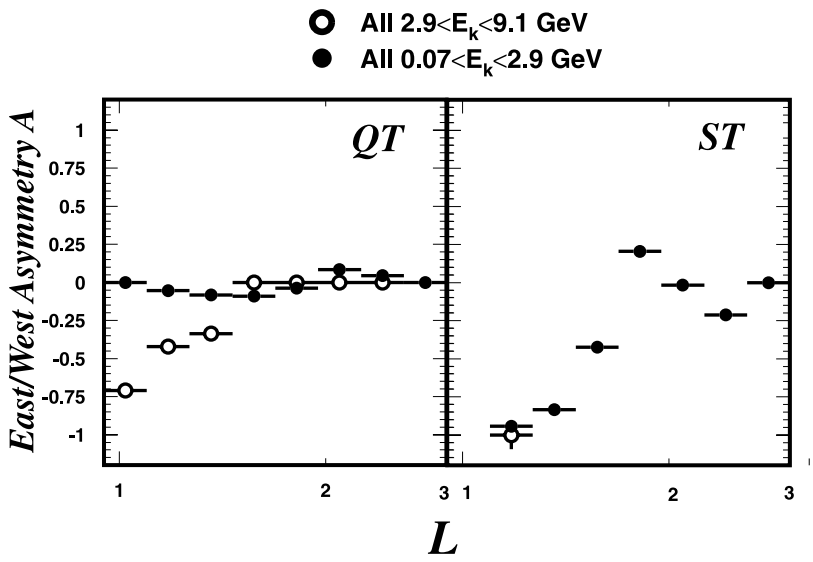

Figure 12. East/west asymmetries for integral flux.

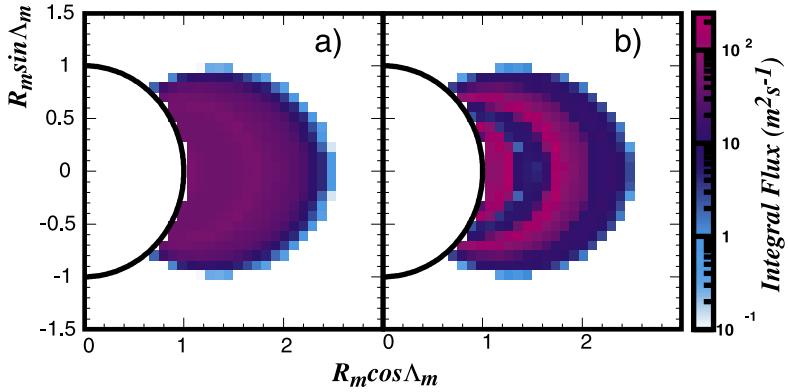

Figure 13. Integral omnidirectional flux maps in (R_m, Λ_m coordinates for (a) QT and (b) ST protons in the full energy interval 0.07–9.1 GeV.

T are large and then westward going particles which experience long-term atmospheric interactions are completely removed.

[38] Integral fluxes for the AMS orbit have been investigated also using the invariant radius and latitude representation, (R_m, Λ_m), which gives the spatial distribution of the particles around the Earth [*Roederer*, 1970]. Each measured pitch angle was converted to the value that would be observed on the same L at a fixed value of $R_m = R_1$. For the AMS circular orbit at R $\sim$ 380 km, a value of R_1 = 1.08 R_E was adopted, close to the upper limit of R_m where only a small fraction of particles mirrors at higher altitude. The flux intensity at R_1 is related to the local intensity by Liouville's theorem and it is given by $j(E, \alpha_1, L, t) = j(E, \alpha, L, t)$ with the new pitch angle α_1 related to the observed α by $\sin^2 \alpha_1 = K \sin^2 \alpha$, with $K = (B_o L^3/BR_1^3)\sqrt{4 - 4R_1/L}$ [*Selesnick et al.*, 1995]. Knowing the flux map at R_1, it is possible to convert the integral radial flux in a (R_m, Λ_m) map. The limiting assumption is that there are no particles with mirror points above AMS altitude. This can bring to an underestimation of the real flux for possible radial diffusion and loss mechanisms. The results are shown in Figures 13a and 13b for QT and ST protons, respectively. It is visible a smooth radial profile for the QT populations. The ST fluxes present a different picture, with a slot region.

4. Conclusions

[39] The AMS measured for the first time with good tracking resolution and high statistics the under cutoff proton fluxes in the energy range 0.07–9.1 GeV at an altitude of 370–390 km. Two populations were distinguished on the basis of the residence time outside the atmosphere: one with residence times not longer than 30 s, called Quasi Trapped (albedo and proper), uniformly distributed along the AMS orbit over the observed energy range, the other with residence times typical of the Van Allen belts, called Stably Trapped, found only in the region nearby the SAA and limited to low energies.

[40] The observations support the existence of a transition region from the Stably Trapped, nearby the SAA, where B < 0.26 G, to the Quasi Trapped populations outside of it. In the transition region the two populations coexist and the fraction of ST flux increases as we move toward the core of the SAA. In the (L, α_0) plane the lower limit is described by the equatorial drift loss cone angle, $\alpha_{st}(L)$, below which no ST particles are found, while the upper limit is given by $\alpha_{IVA}(L)$, above which the ST fraction is the unity.

[41] This region, identified as the proton Mixed Radiation Belt, is a source of the injection and loss of high-energy particles populating the inner Van Allen belts.

[42] The QT fluxes measured inside and outside the SAA present the same features in terms of flux intensity and spatial distribution in the (L, α_0) plane. This indicates that they represent the same population observed on different points of a drift shell.

[43] The residence time of QT particles is very short compared to the typical residence times in the van Allen belts. However, a steady flux of particles is present with an equilibrium between sources, given by secondaries particles produced in the interactions of primary cosmic rays with, and losses, due to absorption in the atmosphere. The residence time of the QT population is determined by the equatorial bouncing loss cone angle, α_b: no Proper QT flux is observed inside this loss cone.

[44] The features of the ST component are different. The ST flux is limited to relatively low energies, detected only in the region of the SAA and displays a radial profile with a minimum between two different regions. This suggests some different process, like Coulomb losses at low L values and radial diffusion at high L values, as indicated by *Jentsch and Wibberenz* [1980].

[45] The Quasi-Trapped component shows appreciable east/west anisotropy only for energies greater than 2.9 GeV. Conversely, for the Stably Trapped flux, clear anisotropies are observed at low L shell values for all the energies.

[46] **Acknowledgments.** We gratefully acknowledge our colleagues in AMS, in particular V. Choutko for his help in the event selection. We greatly benefited from the software libraries (UNILIB, SPENVIS) developed in the context of the Trapped Radiation ENvironment Development (TREND) project for ESTEC, and we thank D. Heynderickx for his help. This work has been partially supported by Italian Space Agency (ASI) under contract ASI I/R/211/00.

[47] Lou-Chuang Lee thanks Minghuey Alfred Huang and Joseph F. Lemaire for their assistance in evaluating this paper.

References

Aguilar, M., et al. (2002), The Alpha Magnetic Spectrometer (AMS) on the International Space Station: Part I—Results from the test flight on the space shuttle, *Phys. Rep.*, *366*(6), 331–405.

Albert, J., G. Ginet, and M. Gussenhoven (1998), CRRES observations of radiation belt protons: 1. Data overview and steady state radial diffusion, *J. Geophys. Res.*, *103*(A5), 9261–9274.

Beutier, T., and D. Boscher (1995), A three-dimensional analysis of the electron radiation belt by the Salammbo code, *J. Geophys. Res.*, *100*(A8), 14,853–14,862.

Esposito, G. (2002), Study of cosmic ray fluxes in low earth orbit (LEO) observed with the AMS experiment, Ph.D. thesis, Ist. Naz. di Fis. Nucl., Perugia, Italy. (Available at http://ams.pg.infn.it/Tesi/tesi_esposito.pdf)

Fiandrini, E., G. Esposito, B. Bertucci, B. Alpat, R. Battiston, W. J. Burger, G. Lamanna, and P. Zuccon (2002), Leptons with $E > 200$ MeV trapped in the Earth's radiation belts, *J. Geophys. Res.*, *107*(A6), 1067, doi:10.1029/2001JA900151.

Fiandrini, E., et al. (2003), Leptons with energy >200 MeV trapped near the South Atlantic Anomaly, *J. Geophys. Res.*, *108*(A11), 1402, doi:10.1029/2003JA009844.

Fung, S. F. (1996), Recent development in the NASA trapped radiation models, in *Radiation Belts: Models and Standards*, *Geophy. Monogr. Ser.*, vol. 97, edited by J. F. Lemaire, D. Heynderickx, and D. N. Baker, pp. 79–91, AGU, Washington, D. C.

Getselev, I. V., et al. (1991), Model of spatial-energetic distribution of charged particles (protons and electrons) fluxes in the Earth's radiation belts (in Russian), *Preprint MGU-91-37/241*.

Gussenhoven, M. S., E. G. Mullen, M. D. Violet, C. Hein, J. Bass, and D. Madden (1993), CRRES high energy proton flux maps, *IEEE Trans. Nucl. Sci.*, *40*, 1450.

Gussenhoven, M. S., E. G. Mullen, and D. H. Brautigam (1996), Phillips Laboratory Space Physics Division radiation models, in *Radiation Belts: Models and Standards*, *Geophys. Monogr. Ser.*, vol. 97, edited by J. F. Lemaire, D. Heynderickx, and D. N. Baker, p. 93, AGU, Washington, D. C.

Heckman, H., and G. Nakano (1963), East-west asymmetry in the flux of mirroring geomagnetically trapped protons, *J. Geophys. Res.*, *68*, 2117.

Hilton, H. H. (1971), *L* parameter: A new approximation, *J. Geophys. Res.*, *76*, 6952–6954.

Huston, S. L., and K. A. Pfitzer (1998), Space environment effects: Low-altitude trapped radiation model, *NASA/CR-1998-208593*, Marshall Space Flight Cent., Huntsville., Ala.

Huston, S. L., G. A. Kuck, and K. A. Pfitzer (1996), Low altitude trapped radiation model using TIROS/NOAA data, in *Radiation Belts: Models and Standards*, *Geophys. Monogr. Ser.*, vol. 97, edited by J. F. Lemaire, D. Heynderickx, and D. N. Baker, p. 119, AGU, Washington, D. C.

Kruglanski, M., and D. Heynderickx (1999), Analysis of the low-altitude proton flux asymmetry: Methodology, *Radiat. Meas.*, *30*, 378–382.

Il'in, V. D., et al. (1986), Stochastic instability of charged particles in a magnetic trap, *Cosmic Res., Engl. Transl.*, *24*, 69–76.

Jentsch, V., and G. Wibberenz (1980), An analytic study of the energy and pitch angle distribution of inner-zone protons, *J. Geophys. Res.*, *85*(1), 1–8.

Lemaire, J., A. D. Johnstone, D. Heynderickx, D. J. Rodgers, S. Szita, and V. Pierrard (1995), Trapped Radiation Environment Model Development: TREND-2 Final Report, *Aeron. Acta*, *393*, 48–51.

Looper, M. D., J. B. Blake, J. R. Cummings, and R. A. Mewaldt (1996), SAMPEX observations of energetic hydrogen isotopes in the inner zone, *Rad. Meas.*, *26*(6), 967–978.

Looper, M. D., J. B. Blake, and R. A. Mewaldt (1998), Maps of hydrogen isotopes at low altitudes in the inner zone from SAMPEX observations, *Adv. Space Res.*, *21*(12), 1679–1682.

McIlwain, C. E. (1961), Coordinate for mapping the distribution of magnetically trapped particles, *J. Geophys. Res.*, *66*, 3681–3691.

Panasyuk, M. I. (1996), Empirical models for terrestrial trapped radiation, *Adv. Space Res.*, *17*(2), 137–145.

Pennypacker, C., G. Smoot, A. Buffington, R. A. Muller, and L. Smith (1973), Measurements of geomagnetic cutoff rigidities and particle fluxes below geomagnetic cutoff near Palestine, Texas, *J. Geophys. Res.*, *78*, 1515–1527.

Ray, E. C. (1962), Reentrant cosmic ray albedo calculation, *J. Geophys. Res.*, *67*, 3289–3291.

Ray, E. C. (1967), An improved reentrant cosmic ray albedo calculation, *J. Geophys. Res.*, *72*, 4839–4844.

Roederer, J. G. (1970), *Dynamics of Geomagnetically Trapped Radiation*, Springer-Verlag, New York.

Sawyer, D. M., and J. I. Vette (1976), The AP8 proton environment for solar max and solar min, *NSSDC/WDC-A-R&S 76-06*, NASA Goddard Space Flight Cent., Greenbelt, Md.

Selesnick, R. S., A. C. Cummings, J. R. Cummings, R. A. Mewaldt, E. C. Stone, and T. T. von Rosenvinge (1995), Geomagnetically trapped anomalous cosmic rays, *J. Geophys. Res.*, *100*, 9503–9518.

Shultz, M., and L. J. Lanzerotti (1974), *Particle Diffusion in the Radiation Belts*, vol. 7, Springer-Verlag, New York.

Tsyganenko, N. A. (1982), Determination of magnetospheric model, *Planet. Space Sci.*, *30*, 985–998.

Verma, S. D. (1967), Measurement of charged splash and re-entrant albedo of the cosmic radiation, *J. Geophys. Res.*, *72*, 915–925.

Vette, J. I. (1991), The NASA/National Space Science Data Center Trapped Radiation Environment Model Program (TREMP) (1964–1991), *NSSDC/WDC-A-R&S 91-29*, NASA Goddard Space Flight Cent., Greenbelt, Md.

Walt, M. (1964), The effects of atmospheric collisions on geomagnetically trapped electrons, *J. Geophys. Res.*, *69*(19), 3947–3958.

Wenzel, K.-P., E. C. Stone, and R. E. Vogt (1975), Splash albedo protons between 4 and 315 MeV at high and low geomagnetic latitudes, *J. Geophys. Res.*, *80*, 3580–3584.

Zuccon, P. (2002), A Monte Carlo simulation of the cosmic rays interactions with the near Earth environment, Ph.D. thesis, Ist. Naz. di Fis. Nucl., Perugia, Italy. (Available at http://ams.pg.infn.it/Tesi/tesi_zuccon.pdf)

Zuccon, P., et al. (2003), Atmospheric production of energetic protons, electrons and positrons observed in near Earth orbit, *Astroparticle Phys.*, *20*, 221–224.

B. Alpat, G. Ambrosi, R. Battiston, B. Bertucci, W. J. Burger, D. Caraffini, L. Di Masso, N. Dinu, G. Esposito, E. Fiandrini, M. Ionica, R. Ionica, M. Menichelli, M. Pauluzzi, and P. Zuccon, Department of Physics, Perugia University, Via Pascoli, 06100 Perugia, Italy. (emanuele.fiandrini@pg.infn.it)